Journal of Materials Chemistry A

PAPER

View Article Online
View Journal | View Issue

Cite this: J. Mater. Chem. A, 2019, 7, 16902

Graphene oxide based dopamine mussel-like cross-linked polyethylene imine nanocomposite coating with enhanced hexavalent uranium adsorption†

Songwei Li,[a] Peipei Yang,[a] Xianhu Liu,*[ab] Jiaoxia Zhang,[cd] Wei Xie,[ce] Chao Wang,[cf] Chuntai Liu[ab] and Zhanhu Guo[bc]

Received 1st May 2019
Accepted 21st June 2019

DOI: 10.1039/c9ta04562g

rsc.li/materials-a

Polydopamine (pDA) self-polymerized from mussel-substance dopamine (DA) induced the grafting of polyethylene imine (PEI) between graphene oxide (GO) interlayers to form the GO-pDA-PEI adsorbent for capturing U(VI). The as-prepared GO-pDA-PEI has a hexavalent uranium (U(VI)) adsorption capacity of 530.6 mg g^{-1}, which is 177% higher than that of pristine GO. Both thermodynamic and kinetic studies indicate a spontaneous and exothermic chemisorption process. The adsorbent demonstrates high adsorption capability and stability even after 5cycles of adsorption–desorption processes. The enhanced U(VI) adsorption capability was due to the unique characteristics of the nanoadsorbent, *i.e.*, the ability to provide enough movement space and highly active sites for the adsorption of U(VI).

1. Introduction

With the rapid development of nuclear energy, a large amount of radioactive wastewater has been discharged into the environment. Hexavalent uranium (U(VI)) as the main component of radioactive wastewater poses a considerable hazard to human health and ecological systems. Meanwhile, the exploitation of seawater uranium extraction technology becomes the most promising and feasible way to obtain large amounts of uranium resources. Hence, extraction of U(VI) from various radioactive wastewater and seawater sources is of scientific and practical significance.[1–3] Compared with the reported methods of adsorbing U(VI) from radioactive wastewater including electrodialysis, extraction, chemical precipitation, and organic–inorganic ion exchange,[4,5] adsorption is more favourable since it is a flexible and simple technology with highly efficient U(VI) removal.[6] However, traditional adsorbing materials suffer from low capability and poor selectivity for U(VI) adsorption from aqueous solutions. Thus, preparing an efficient adsorbent with high adsorption capability, high selectivity and suitable pH for wastewater and seawater is a great challenge.

Graphene oxide (GO), a 2D material, has attracted increasing attention as an adsorbent due to its rich adsorption sites and hydrophilic character. For example, Li *et al.* described hypha/GO as a convenient material for the adsorption of U(VI).[7] Liu *et al.* prepared attapulgite–GO composites for efficient uranium adsorption.[8] Lingamdinne *et al.* studied the enrichment of uranium by GO based inverse spinel nickel ferrite.[9] Bovine serum albumin and UiO-66 were successfully grafted onto carboxyl functional groups on the GO surface *via* condensation and coordination and demonstrated both enhanced uranium adsorption and improved selectivity.[4,18] However, the compensation for the lost active sites arising from the irreversible coagulation of the GO layer spacing remains a big challenge.

A chemical post-decoration strategy has shown crucial promise for the preparation of GO-based materials, which can reduce the van der Waals force of the layer spacing and release a large number of active sites for increasing the selectivity and adsorption capacity for U(VI). Previous studies suggested that GO modified with organic functional groups such as amines, hydroxyls or carboxylic acids would provide abundant binding sites in the interface of GO.[10–12] Polyethyleneimine (PEI) as a polymer with rich amine groups per chain is frequently used to decorate the surface of nanomaterials.[13] Dopamine (DA), an organic substance inspired by mussels from the ocean, is an excellent adhesive organic substance containing a large number of amine and hydroxy groups.[14] The mussel-inspired adhesive organic compound not only forms a ketone by oxidative self-polymerization for the Schiff base reaction of amines, but also

[a]National Engineering Research Center for Advanced Polymer Processing Technology, Zhengzhou University, Zhengzhou 450002, China. E-mail: xianhu.liu@zzu.edu.cn
[b]Key Laboratory of Materials Processing and Mold (Zhengzhou University), Ministry of Education, Zhengzhou 450002, China
[c]Integrated Composites Laboratory (ICL), Department of Chemical & Biomolecular Engineering, University of Tennessee, Knoxville, TN 37996, USA
[d]School of Material Science and Engineering, Jiangsu University of Science and Technology, Zhenjiang, Jiangsu, 212003, China
[e]Key Laboratory of Lightweight and Reliability Technology for Engineering Vehicle, Education Department, Changsha University of Science & Technology, Changsha, China
[f]School of Materials Science and Engineering, North University of China, Taiyuan 030051, China

† Electronic supplementary information (ESI) available. See DOI: 10.1039/c9ta04562g

provides an active intermediate layer to improve the loading rate and stability among various base materials (such as MOFs, nanosilica, carbon materials, GO, polymers *etc.*).[15–18] Note that the amines from DA form covalent bonds with carboxyl groups on the GO surface to enhance the stability of the material. This provides enough movement space and active sites for the GO sheets to adsorb much more U(VI). However, there are few research studies about PEI modification on GO nanosheets by a green one-step synthesis.

Herein, a U(VI) adsorption coating was introduced on the graphene oxide surface by an organic substance-induced strategy. Dopamine (DA) and PEI were grafted to GO with different ratios to achieve a high efficiency and high adsorption capacity. The layer spacing of GO was found to change with the change of the PEI amount and thus influenced the adsorption. The composites not only compensated the lost active sites arising from the irreversible coagulation of the GO sheets but also provided enough movement space and active sites for absorbing U(VI). The chemical stability and adsorption performance of the adsorbents were significantly improved. The detailed effects of parameters on the U(VI) adsorption behaviour were studied including pH, the initial concentration of U(VI), adsorption kinetics, adsorption isotherms and ionic competition. These results illustrated that carboxyl groups, hydroxyl groups and amine groups should be responsible for the high selectivity and adsorption capacity for U(VIVI).

2. Experimental

2.1 Adsorbent preparation

All the materials were used as received without any further treatment.

GO-pDA-PEI. 200 mg GO prepared by modified Hummers' method[19–21] and 50 mg dopamine were added to 10 mL Tris buffer and sonicated for 30 s. Then 50 mg PEI was added to the above solution and stirred for 3 hours. The material was then placed in a freeze-drying box for 72 h freeze-drying. The sample was denoted as GO-pDA-PEI. The synthetic route is shown in Scheme 1.

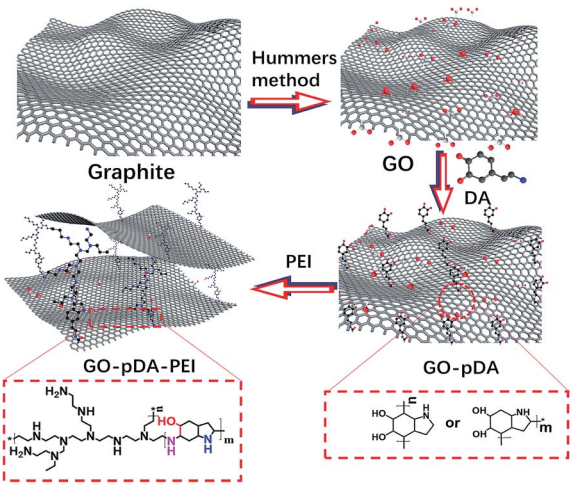

Scheme 1 Proposed schematic diagram of the synthesis of the GO-pDA-PEI material.

GO-pDA. GO (200 mg) and dopamine (50 mg) were added to 10 mL Tris buffer and sonicated for 30 s. After the mixing was complete, the solution was placed in a shaking table for 1 h. Then, the reaction solution was dried for 72 h. The sample was denoted as GO-pDA.

2.2 Characterization

The morphologies of GO, GO-pDA and GO-pDA-PEI were observed by using an FEI Tecnai G2 S-Twin transmission electron microscope (TEM). X-ray diffraction (XRD) analysis was performed on a Rigaku TTR-III diffractometer with Cu K_α irradiation under the conditions of $K_\alpha = 1.54178$ Å, $U = 40$ kV and $I = 150$ mA. An ESCALAB 250Xi X-ray photoelectron spectrometer (XPS) was employed to detect the elements in the samples. An Avatar 370 FTIR was used to confirm the successful assembling of the samples.

2.3 Adsorption experiments

0.01 g GO, GO-pDA or GO-pDA-PEI composites were added into $UO_2(NO_3)_2 \cdot 6H_2O$ aqueous solution (20 mL). After oscillation adsorption in a conical flask, these solutions were separated by centrifugation. The remaining U(VI) ion concentrations from aqueous solution were tested by ICP-AES using an IRIS Intrepid II XPS. During this experiment, 0.1 M HNO_3 and 0.1 M Na_2CO_3 were employed to adjust the pH. The total adsorbed U(VI) per mass of the adsorbent was computed using eqn (1):[22]

$$q_e = (C_o - C_e) \times V/m \quad (1)$$

where C_o (mg L^{-1}) and C_e (mg L^{-1}) represent the original and equilibrium concentrations of U(VI), respectively; q_e represents the adsorption amount, V (L) refers to the volume of the solution and m (g) refers to the mass of the adsorbent.

3. Results and discussion

3.1 Morphological performance

For GO, the strong and broad adsorption band at 3300 cm^{-1} is attributed to the stretching vibration of the associated –OH on the GO nanoplatelets. The strong and sharp adsorption band at 1700 cm^{-1} belongs to the stretching vibration of C=O in the carboxyl groups. The stretching vibration peaks at 1650 and 1500 cm^{-1} are caused by the skeleton vibration of the benzene ring on the GO.[23] Compared to the FT-IR spectrum of GO, the symmetric and asymmetric stretching vibration peaks of methylene at 2800 and 2900 cm^{-1} together with the occurrence of benzene ring substitution peaks at 804 and 898 cm^{-1} show the successful introduction of pDA into the GO interface.[24] In the FT-IR spectrum of GO-pDA-PEI, the appearance of the stretching vibration peaks of secondary amine groups at 615 and 719 cm^{-1} indicates that PEI has been successfully decorated on the GO-pDA interface.[25] The shearing vibration peak observed at 1519 cm^{-1} belongs to –N–H of the amide group.[26] The peak at 2269 cm^{-1} belongs to –NCO antisymmetric

stretching.[27] In addition, the new peak of GO-DA and GO-DA-PEI composites at 630 cm^{-1} is related to the in-plane bending vibration of O=C–NH.[4] Fig. 1a summarizes the above FTIR spectral analysis.

The evolution of the crystal structure of GO after introducing pDA and PEI was monitored by XRD, Fig. 1b. A sharp and strong peak at 11.4° and a weak and broad peak at 22.5° correspond to the 100-plane and 002-plane of GO, respectively. Compared to those of GO, the 100-plane and 002-plane peaks of GO-pDA move to lower degrees. According to the Bragg equation, the layer spacing of GO increases, indicating that DA has been successfully inserted into the GO layer spacing.[28] For GO-pDA-PEI, the peak at 11.0° is weaker than that of GO and GO-pDA, and the peak at 20.0° becomes a broad medium-strong peak, demonstrating that PEI further changes the layer spacing of GO-pDA.

In Fig. 1c, the BET surface areas of GO, GO-pDA and GO-pDA-PEI are 963.53, 768.83 and 598.92 $m^2\ g^{-1}$, respectively. As GO was further functionalized by DA and PEI, the BET surface area decreased. This could be ascribed to a large amount of pDA and PEI that was coated successfully on the surface of GO.

Fig. 2a shows the wrinkled and thin layered structure of GO. Compared with GO, GO-pDA (Fig. 2b) retains its morphology unchanged and the thickness of the GO sheet increases, indicating a small amount of organic matter on the edge of GO. This phenomenon proves that pDA was successfully grafted onto the GO nanosheets and the original structure of GO was maintained. From Fig. 2c, it can be seen that the layered structure of the GO-pDA-PEI material is increased relative to the thickness of GO-pDA. In order to further study its surface structure, the element distribution on its surface is studied, as shown in Fig. 2c and partially enlarged Fig. 2c. The elements C, O and N are detected in all regions. This indicates that both PEI and DA can achieve the purpose of modifying GO.

3.2 Adsorption studies

The adsorption behaviors of GO, GO-pDA and GO-pDA-PEI composites were tested for U(VI) adsorption, and the best ratio was screened in the work. From Table S1 in the ESI,† it is clear that adsorption reaches the highest when the mass ratio of DA : PEI is 2 : 2. This result indicates that an appropriate ratio of DA/PEI not only increases the active sites on the GO surface, but also regulates an appropriate layer spacing for capture of U(VI) by GO-pDA-PEI. Therefore, in the following study, the mass ratio of DA and PEI in GO-pDA-PEI was 2 : 2.

pH is a key factor that influences U(VI) ion adsorption. Compared to GO and GO-pDA, the U(VI) adsorption capacity of GO-pDA-PEI increased with increasing the pH value from 2 to 5, due to the fact that DA and PEI activated more available sites for binding U(VI) ions. Moreover, as the concentration of H^+ ions is reduced with the increase of the pH, more effective sites on the surfaces of adsorbents are released. Remarkably, as the pH rises from 5 to 9, GO-pDA-PEI exhibits good pH responsiveness. This phenomenon makes GO-pDA-PEI have broad applications in U(VI) extraction. In addition, in the optimal pH of 5, the predominant uranium form is UO_2^{2+} for GO-pDA-PEI, indicating that GO-pDA-PEI has a high coordinating capacity for UO_2^{2+}. Based on the above information, pH = 5 was selected for the following experiments. Then, different initial concentrations of U(VI) were chosen to further test different adsorbents. From Fig. 3b, the adsorption capacity of each adsorbent is observed to increase significantly with increasing the U(VI) concentration from 50 to 600 mg g^{-1}. Importantly, GO-pDA-PEI composites show a higher adsorption capacity than others, indicating that more active sites of GO-pDA-PEI are available for adsorption.

3.3 Adsorption kinetics and adsorption isotherms

The adsorption kinetics of GO-pDA and GO-pDA-PEI was investigated and shown in Fig. 4a. These graphs display that the adsorption capacity shows a sharp upsurge with time until reaching an equilibrium, and the adsorption capability of GO, GO-pDA and GO-pDA-PEI is 299.7, 314 and 416 mg g^{-1}, respectively. The adsorption equilibrium time of GO-pDA and GO-pDA-PEI is shorter than that of GO. It is clear that the adsorption efficiency of GO-pDA-PEI was higher than that of GO. This is due to the increased interlayer spacing between PEI and pDA to promote the flow of the aqueous solution.

Pseudo-first-order, pseudo-second-order and Weber–Morris (W–M) models (refer to the ESI† for details) were used to study the dynamic processes. The data in Fig. 4b, c and Table S2† demonstrate that GO-pDA and GO-pDA-PEI follow a pseudo-second-order model ($R_{GO}^2 = 0.99917$, $R_{GO\text{-}pDA}^2 = 0.99989$, and $R_{GO\text{-}pDA\text{-}PEI}^2 = 0.99982$), indicating chemisorption as the main controlling

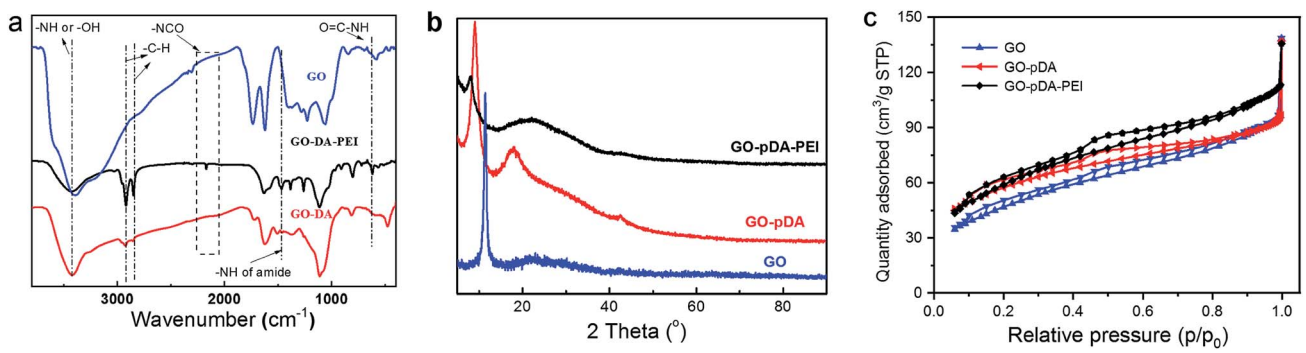

Fig. 1 (a) FT-IR spectra, (b) XRD patterns and (c) N_2 adsorption–desorption isotherms of GO, GO-pDA and GO-pDA-PEI composites.

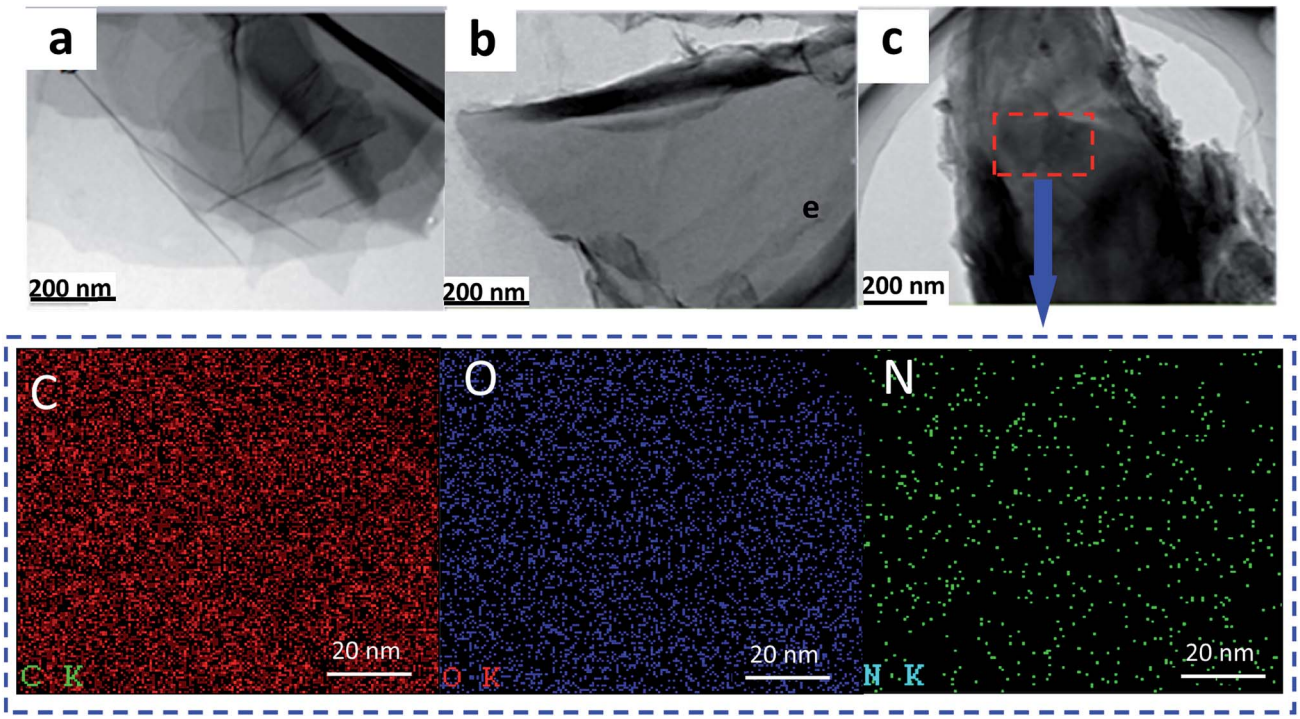

Fig. 2 TEM of GO (a), GO-pDA (b) and GO-pDA-PEI (c); and the corresponding elemental C, O and N mapping of the GO-pDA-PEI nanocomposites.

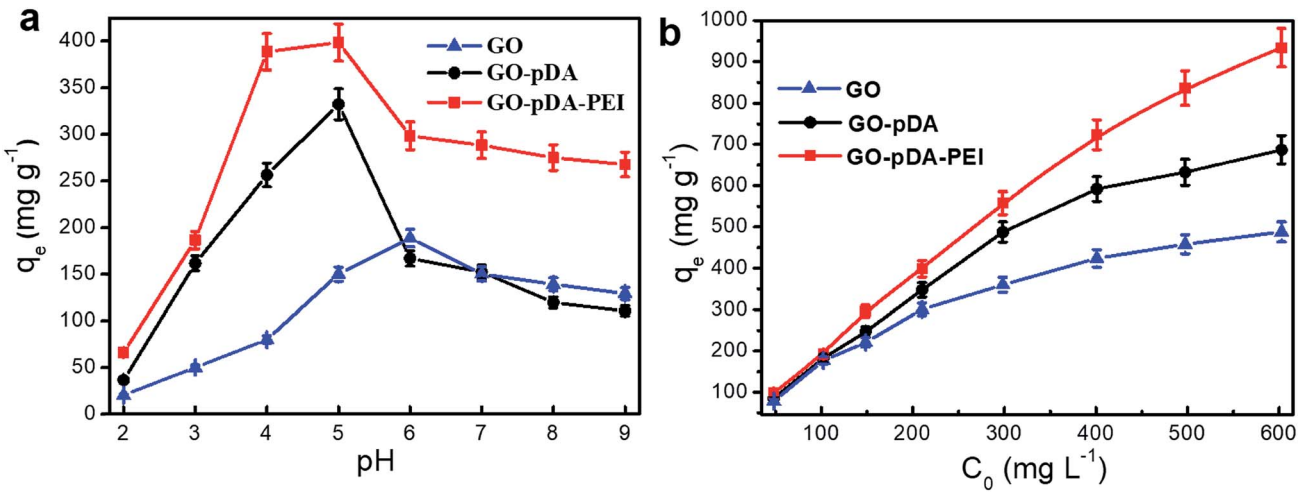

Fig. 3 Effect of (a) pH and (b) initial U(VI) concentration on the adsorption properties of GO, GO-pDA and GO-pDA-PEI composites.

step. In other words, the adsorption rate relies on the rate of coordination of U(VI) ions onto the interface of these materials. For the W–M model (Fig. 4d), the C value reflects the influence of the boundaries of adsorbing materials on U(VI) adsorption. A larger C value represents a greater contribution from the periphery of adsorbing materials. In Table S3,† the C values of surface adsorption and slow diffusion of pores for GO, GO-pDA and GO-pDA-PEI are 22.8, 270.9, 252.4, 304.05, 194.48 and 410.25, respectively, illustrating that the boundary of adsorbing materials has a greater influence on the process of U(VI) adsorption. In the first-phase of intra-particle diffusion (Table S3, ESI†), the K_{ip} (internal diffusivity constant) values for GO, GO-pDA and GO-pDA-PEI are 73.4, 12.2 and 41.3, which suggest that GO-pDA-PEI has a higher diffusion rate than GO and GO-pDA. Besides, the fitting curve did not pass through the original point, indicating that the external diffusion controls the entire adsorption process. In the second-step (Table S3†), the K_{ip} values of GO, GO-pDA and GO-pDA-PEI are 2.08, 1.94 and 0.14, revealing lower rates compared to the first-step. In addition, the intercept of fitting curves is close to 0, indicating that the intra-particle diffusion is the major rate-determining phase in this step, and the greater boundaries have a tiny contribution. Generally, the adsorption

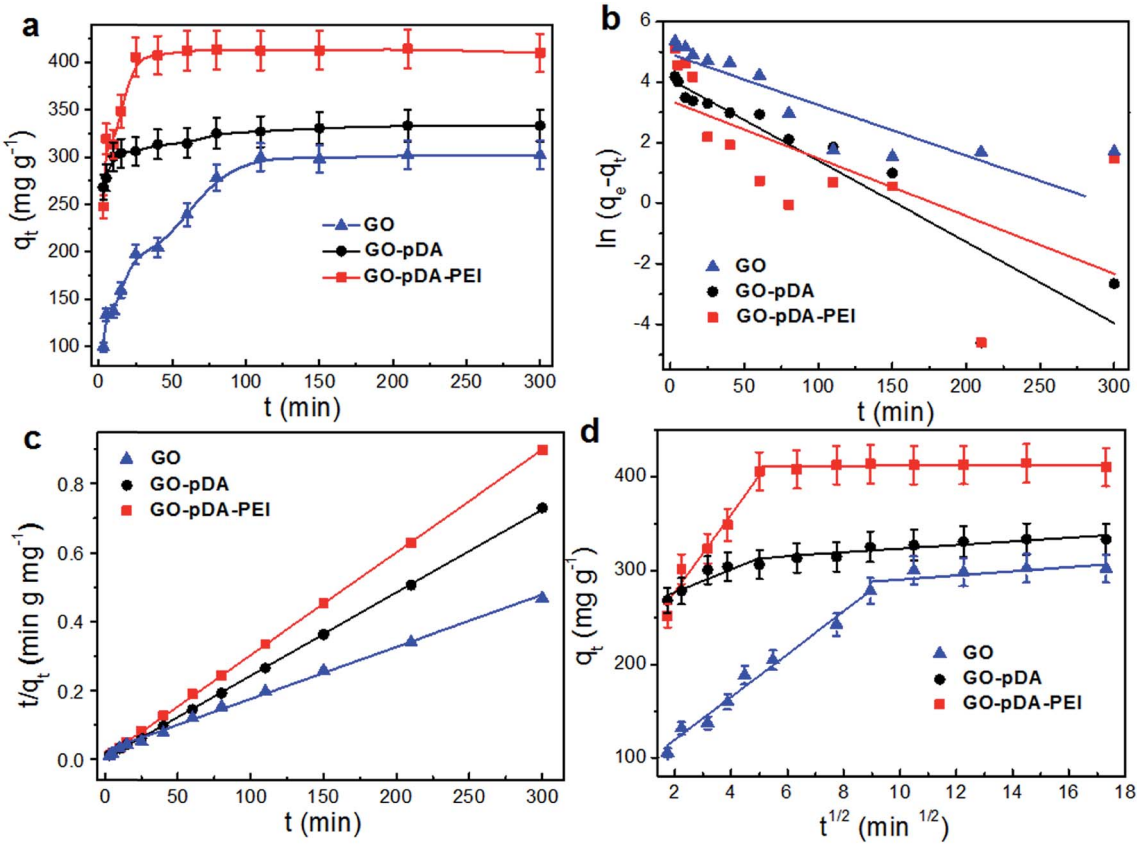

Fig. 4 Effect of contact time (a), pseudo-first-order (b), pseudo-second-order (c) and Weber–Morris model (d) on the adsorption properties of GO, GO-pDA and GO-pDA-PEI composites, pH = 5.00; T = 25 °C; amount of adsorbent 0.01 g and U(VI) = 210 mg L^{-1}.

behaviour of U(VI) on GO-pDA-PEI consists of two parts. The first part is the coordination or electrostatic interaction of the nitrogen- and oxygen-containing organic units on the edges of the adsorbent with U(VI). In the second part, U(VI) enters into the interlay due to the intra-particle diffusion leading to a further improvement of the adsorption capacity.

In order to explain the adsorption behaviour of U(VI) on the adsorbent surface and adsorption capacity of the adsorbent at the setting temperature, herein, Langmuir and Freundlich models were employed,[29] as shown in Fig. 5, S1 and Table S4.† From these data, the isotherm follows the Langmuir model (R_{GO}^2 = 0.99887, $R_{GO\text{-}pDA}^2$ = 0.99558, and $R_{GO\text{-}pDA\text{-}PEI}^2$ = 0.98551) instead of the Freundlich model (R_{GO}^2 = 0.92893, $R_{GO\text{-}pDA}^2$ = 0.72233 and $R_{GO\text{-}pDA\text{-}PEI}^2$ = 0.89026), which indicates the existence of an evenly chemisorped monolayer.

Based on the above isotherm findings, the thermodynamics governing the adsorption of U(VI) on adsorbents was examined. Equalities S6–S8† were used to analyze the thermodynamic issues. In Fig. S2,† the adsorption capacity decreases when the temperature rises, indicating an exothermic adsorption process. ΔG^o < 0 (Table S5†) shows that U(VI) adsorption is spontaneous.

3.4 Recyclability of adsorbents

The reutilization of adsorbents was tested by the capture of U(VI) from aqueous solution. In Fig. 6, the elution efficiency of GO-pDA-PEI is observed to be comparatively high after five cycles (91–80%), which indicates that it is a good adsorbing material to capture U(VI) in solution. The almost same XRD patterns (Fig. S3†) as those of the freshly prepared adsorbents show the stability of the GO-pDA-PEI composites after 5 cycles. From Fig. S4,† it is clear that the eluent rate of the adsorbent decreases as the number of repetitions increases. Correspondingly, the eluent rates of adsorbents decrease as the number of repetitions increases, most likely owing to the adsorbent's mass loss and partly due to the non-renewable active sites. With the increase of cycle times, the mass loss of the adsorbent becomes less and less, which indicates that the prepared adsorbent has a good stability. In this process, 0.8 M NaCl was used as the eluent (the detailed information is shown in Tables S6 and S7†). To sum up, GO-pDA-PEI exhibits an unexpected potential for the extraction of U(VI) from solutions.

3.5 Co-existing ion test and simulated seawater testing

The presence of many other metal cations in industrial wastewater or seawater may affect the adsorption of uranyl ions. A series of cationic competition experiments have been explored, as shown in Fig. 7a and b. GO-pDA-PEI shows excellent selectivity compared to GO and GO-pDA with an unexpected removal rate of over 95% under the influence of co-existing ions. Besides, the result shows that Cu^{2+} and Ba^{2+} have a higher effect than Ni^{2+}, Mg^{2+}, and Ca^{2+} for U(VI) adsorption. The selective

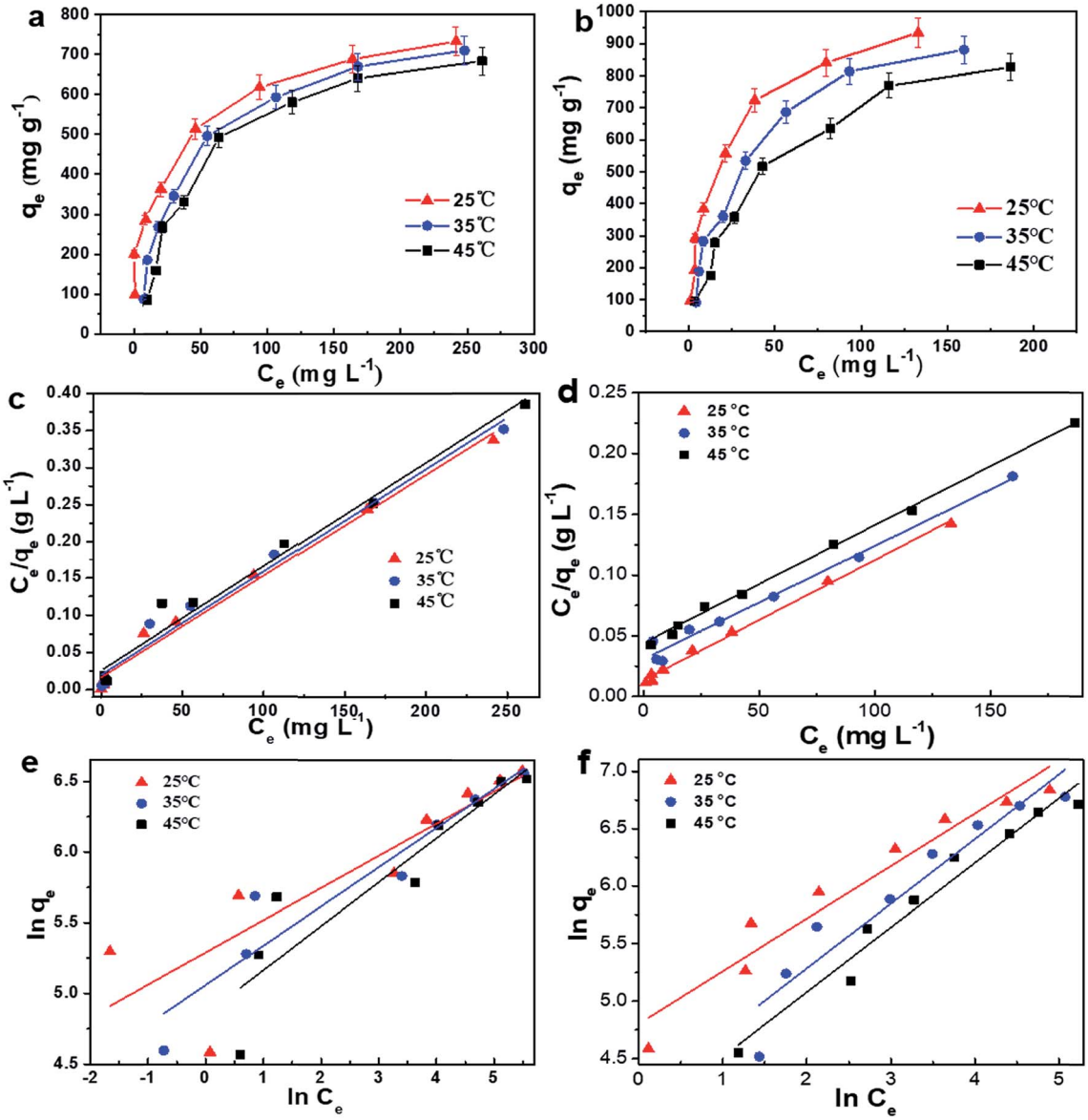

Fig. 5 Isotherm model for (a) GO-pDA and (b) GO-pDA-PEI composites; Langmuir model for (c) GO-pDA and (d) GO-pDA-PEI composites; Freundlich model for (e) GO-pDA and (f) GO-pDA-PEI composites.

change is presumed to contribute to the adsorption of metal ions onto the outside of GO-pDA-PEI.[30] Cu^{2+} and Ba^{2+} easily form hydroxides and generate sediments that should be just physically adsorbed surrounding the edge of the adsorbent.[31] However, the adsorption of U(VI) onto the adsorbent involves mostly chemical adsorption, triggering these ions to have a minor power compared to other ions on the selectivity of adsorption. Interactions occur between Ni^{2+}, Mg^{2+}, and Ca^{2+} and the amino fragments of GO-pDA-PEI. They create less unsteady complexes than Ba^{2+} and Cu^{2+}.

Meanwhile, the U–N bond length is longer than that formed by uranyl ions with Zn^{2+}, Mg^{2+}, Al^{3+} and Fe^{3+}, indicating that the combination of nitrogen and uranyl ions is greatly affected by these metal ions (Zn^{2+}, Mg^{2+}, Al^{3+} and Fe^{3+}). The U–N bond is shorter than the bond length of uranyl ions with other metals (K^+, Na^+, Ca^{2+}, Ba^{2+}, Cu^{2+}, Ni^{3+}, Pb^{2+}, Mn^{2+}, and Sr^{2+} ions). This suggests that U(VI) has a more stable bond with the amino group, so that nitrogen has a greater affinity for uranyl ions than these ions.[32] Besides, uranyl ions can be seen as hard acids and can form coordinate bonds with hard bases. Some studies also illustrated that functional groups containing hard bases grafted to the surface of the material can form stable coordination with U(VI).[33] For example, Liu *et al.* revealed that stable –COOH can be obtained during adsorption of U(VI).[34] Li *et al.* also proved that U(VI) interacted with $-NH_2$ during the removal of U(VI).[35] Taking into account the adsorption of other metal ions, the adsorption capacity is largely influenced by Cu^{2+} and Ba^{2+} in solvent. This finding can be confirmed from the distribution coefficient (K_d) of U(VI) in Fig. 7a and extra background metal ions. It is clear that the K_d of U(VI) (K_d^U) is higher than that of other ions, which

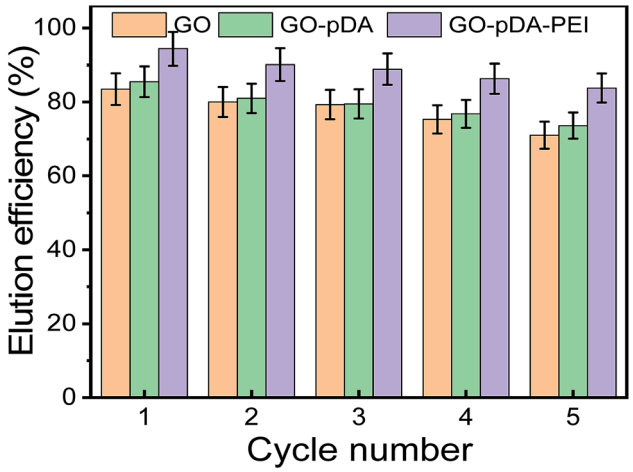

Fig. 6 Desorption and renewable cycles of GO, GO-pDA and GO-pDA-PEI composites.

suggests that GO, GO-pDA and GO-pDA-PEI have a very good binding ability to uranium. The outstanding higher value of K_d^U of GO-pDA-PEI (nearly 100 000), compared with the K_d^U of GO (nearly 12 000) and K_d^U of GO-pDA (nearly 20 000), means that GO-pDA-PEI has an excellent binding performance for U(VI).

In addition, the selectivity coefficient of U(VI) (S_U) divided by that of other metal ions is shown in Table S8.†[36] The data of $S_{U/M}$ in Table S8† show the great selectivity of GO-pDA-PEI toward U(VI) in the case of various co-existing metal ions, especially for Ni^{2+}, Mg^{2+}, and Ca^{2+}. To sum up, these results indicated that GO-pDA-PEI has an excellent binding ability to U(VI) in complex aqueous solutions.

The GO-pDA-PEI adsorbent was further investigated to discuss its selectivity for U(VI) and adsorption abilities. In the experiment, simulated seawater is prepared as shown in ESI.3.† The pH value of different U(VI) concentrations in simulated seawater is listed in Table S9† and ion species in Table S10.† The adsorbent was soaked in simulated seawater contaminated with uranium concentrations of 3.35 μg L^{-1}, 5.86 μg L^{-1}, 9.52 μg L^{-1}, 16.8 μg L^{-1}, 50.5 μg L^{-1} and 98.1 μg L^{-1}. The results indicated that all of the removal rates for U(VI) are more than 90% (Fig. 7d) for GO-pDA-PEI, which means that the GO-pDA-PEI adsorbent has an excellent adsorption capacity for removal of uranium from seawater. The data about GO-pDA-PEI can provide several theoretical ideas for U(VI) capture from natural seawater.

3.6 Mechanism of adsorption

The adsorption behavior of U(VIVI) on GO-pDA-PEI has been discussed through studying the effects of pH, kinetics and adsorption isotherms. To further explain the adsorption

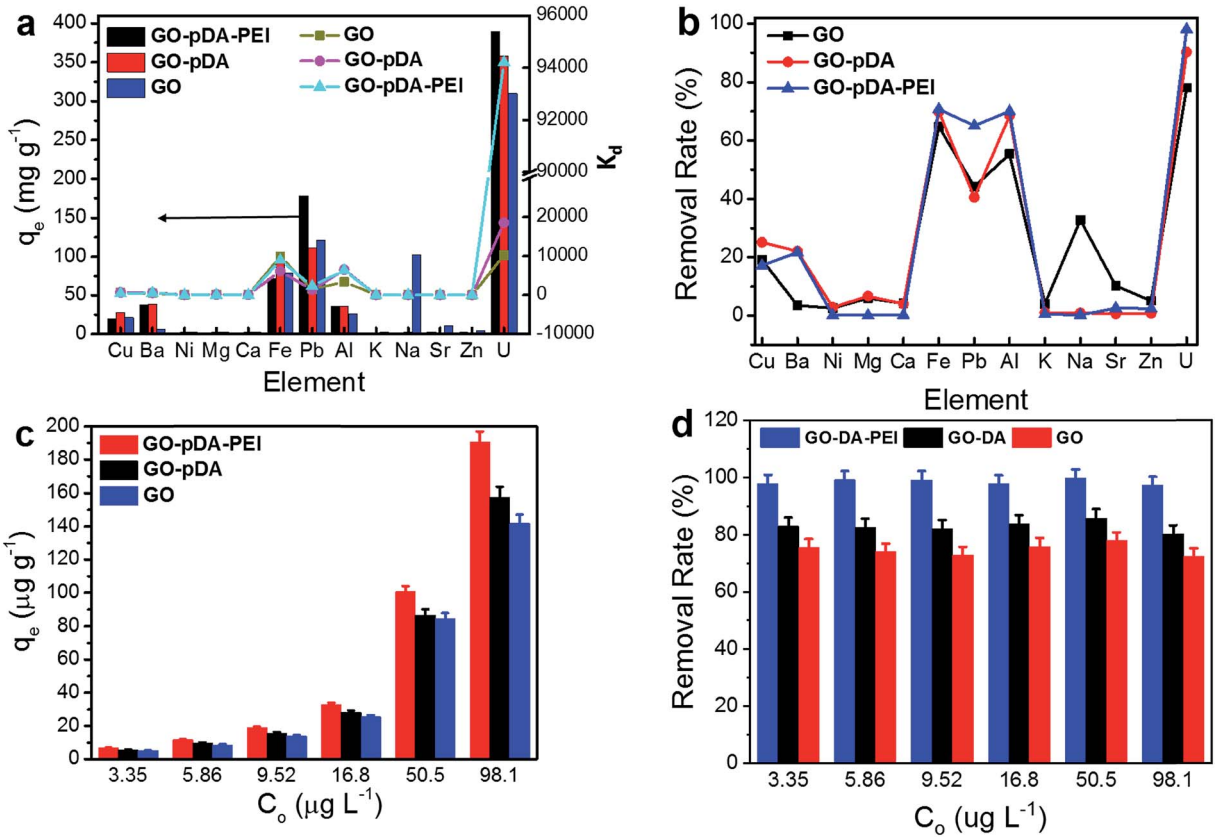

Fig. 7 (a) The adsorption capacity of GO, GO-pDA and GO-pDA-PEI for various ions and their K_d values and (b) removal rate of GO, GO-pDA and GO-pDA-PEI; effect of (c) initial concentration of U(VI) on its adsorption capacity from simulated seawater and (d) the removal rate under different concentrations of U(VI) at almost the same pH.

mechanism of U(VI) onto the surfaces of GO-pDA-PEI, XPS and FTIR were used. From the survey spectra of XPS (Fig. 8a), U(VI) is observed to be successfully adsorbed onto the surface of the adsorbent. Besides, the binding energy of N 1s and O 1s peaks after the adsorption of U(VI) becomes lower than that of the peaks before adsorption. It is obviously revealed that the U(VI) adsorption performance of GO-pDA-PEI may depend on the oxygen- and nitrogen-containing organic groups.[37] Importantly, the change of O 1s (~0.38 eV) binding energy is lower than that of N 1s (~0.90 eV) of GO-pDA-PEI, indicating that $-NH_2$ and –NH on the surface of the material are coordinated with U(VI).[19,38–40] From the O 1s peak in Fig. S5 (ESI†), it can be seen that the peak area of –OH changes after the adsorption of U(VI) on GO-pDA-PEI, while the peak area of –O– has no obvious change. This indicates that the carboxyl group and hydroxyl group of GO-pDA-PEI have strong coordination with uranium, while the epoxy group does not participate in adsorption.

In the FT-IR spectrum of GO-pDA-PEI after U(VI) adsorption , the bands at 3400, 630 and 729 cm^{-1} display a blue shift, which gives a clear indication of the interaction between U(VI) and

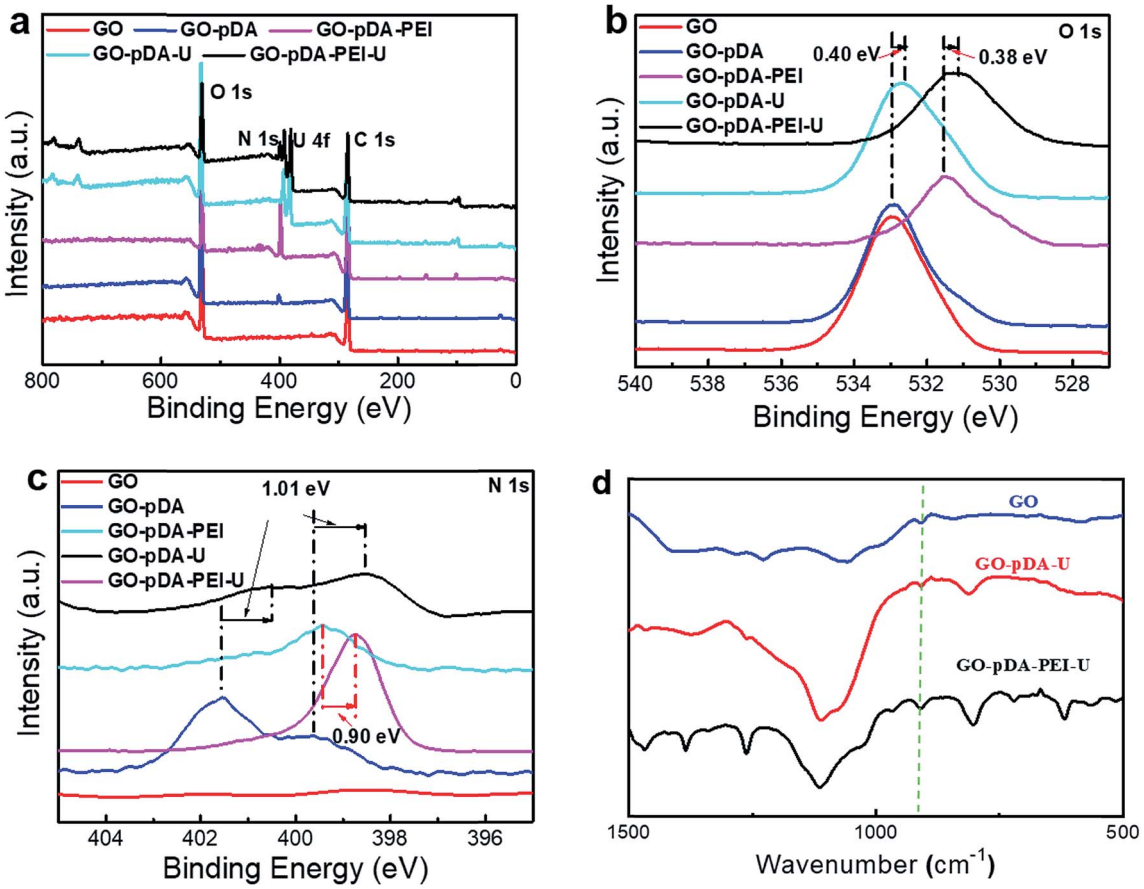

Fig. 8 (a) XPS survey spectra after adsorption of U(VI) onto GO, GO-pDA and GO-pDA-PEI, (b) O 1s and (c) N 1s patterns after adsorption of U(VI) onto GO, GO-pDA and GO-pDA-PEI, (d) FTIR spectra after adsorption of U(VI) onto GO, GO-pDA and GO-pDA-PEI.

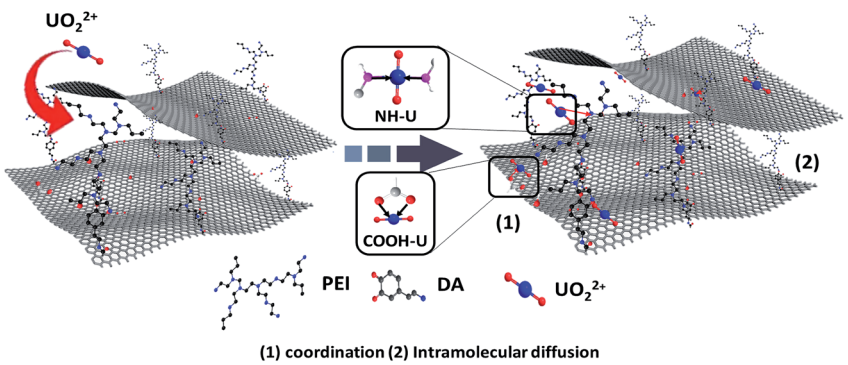

Scheme 2 Proposed adsorption mechanism of GO-pDA-PEI.

Table 1 Comparison of the adsorption capacity of GO-pDA-PEI with that of reported GO from the literature

Adsorbents	q_{max} (mg g^{-1})	C_o (mg L^{-1})	m/V (g L⁻1)	pH	Ref.
Graphene oxide-cellulose	101.01	10	1.75	4	42
Binary ferberite-graphene	410	300	0.3	6	43
Graphene oxide/polyethyleneimine	629.5	300	0.4	5	18
Fungal hypha/graphene oxide	288.42	120	0.33	5	7
Attapulgite and graphene oxide	8	10	1	5	8
Graphene oxide/Ni–Al LDH	277.8	150	0.5	4	44
Graphene oxide/MnO_2	66.8	45	0.25	4	45
Magnetic cucurbituril/graphene oxide	122.5	36	0.2	5	46
GO-pDA-PEI	198.6	100.3	0.5	5	Present study
GO-pDA-PEI	416	209.6	0.5	5	Present study
GO-pDA-PEI	530.6	300.2	0.5	5	Present study

–OH, –NH.[3,41] After the adsorption of U(VI) on GO-pDA-PEI, the band at 920 cm^{-1} is caused by the asymmetric stretching vibration of O═U═O. Additionally, the intensity of the peak at 920 cm^{-1} was enhanced obviously due to the interaction between the adsorbed O═U═O and the adsorbent of GO-pDA-PEI. This indicates that the FT-IR results are consistent with XPS analysis. The N_2 adsorption–desorption isotherms of GO, GO-pDA and GO-pDA-PEI composites after adsorption (Fig. S6 and Table S11†) show that the specific surface area decreased after the adsorption of U(VI). This may be due to the occupation of active sites on the surface of the material by the introduced uranium. To sum up, a possible adsorption mechanism of U(VI) on GO-pDA-PEI is shown in Scheme 2.

3.7 Comparison of the adsorption capacity of GO-pDA-PEI with that of graphene oxide-adsorbents

Compared with the reported adsorbents, GO-pDA-PEI displays excellent adsorption efficiency (Table 1). The adsorption capacity of GO-pDA-PEI is 198.6 mg g^{-1} (pH = 5.0, C_o = 100.3 mg L^{-1}) and 530.6 mg g^{-1} (pH = 5.0, C_o = 300.2 mg L^{-1}), which are larger than that of most of other adsorbents. Compared to the work reported by Shi *et al.*,[18] the adsorption amount of GO-pDA-PEI (530.6 mg g^{-1}) is a little lower than that of GO-PEI. But, the adsorbing materials reported in this work showed a good adsorption selectivity under ion competition and simulated seawater conditions. In the ion competition experiment, the removal rate of the materials is 95.8%, which is higher than the reported results. The removal rate in the simulated seawater is above 90% (Fig. 7c and d). Furthermore, the adsorbents demonstrated superior removal efficiency and stability even after 5 cycles of adsorption–desorption processes.

4. Conclusions

In conclusion, GO-pDA-PEI was prepared through an organic substance-induced synthesis strategy. The mussel-substance-induced PEI grown on graphene oxide (GO) provided enough movement space and active sites for GO sheets to adsorb much more U(VI). The adsorbent followed the pseudo-second-order model, Morris–Weber (M–W) model and Langmuir model. Besides, GO-pDA-PEI exhibited excellent adsorption capacity (530.6 mg g^{-1}, pH = 5), greater ionic selectivity and good kinetics. The regeneration of the absorbent was validated by five cycles, and the removal efficiency of GO-pDA-PEI remained at 80%. Also, GO-pDA-PEI exhibited a great stability. Importantly, from the FTIR and XPS analyses of GO-pDA-PEI before and after the adsorption of U(VI), the enhanced adsorption performance was ascribed to the chelation of U(VI) with the carboxyl and amino groups of GO-pDA-PEI. We can conclude that the materials have unexpected potential as preeminent adsorbents to capture U(VI) from wastewater and seawater.

Conflicts of interest

There are no conflicts to declare.

References

1 (*a*) A. Dong, Y. Zhu, M. Ren, X. Sun, V. Murugadoss, Y. Yuan, J. Wen, X. Wang, Q. Chen, Z. Guo and Z. Guo, *Eng. Sci.*, 2019, **6**, 44–52; (*b*) J. Li, X. Wang, G. Zhao, C. Chen, Z. Chai, A. Alsaedi, T. Hayat and X. Wang, *Chem. Soc. Rev.*, 2018, **47**, 2322–2356.
2 X. Wang, Y. Liu, H. Pang, S. Yu, Y. Ai, X. Ma, G. Song, T. Hayat, A. Alsaedi and X. Wang, *Chem. Eng. J.*, 2018, **344**, 380–390.
3 Z. Huang, Z. Li, L. Zheng, L. Zhou, Z. Chai, X. Wang and W. Shi, *Chem. Eng. J.*, 2017, **328**, 1066–1074.
4 P. Yang, Q. Liu, J. Liu, H. Zhang, Z. Li, R. Li, L. Liu and J. Wang, *Ind. Eng. Chem. Res.*, 2017, **56**, 3588–3598.
5 Y. Zou, X. Wang, Y. Ai, Y. Liu, Y. Ji, H. Wang, T. Hayat, A. Alsaedi, W. Hu and X. Wang, *J. Mater. Chem. A*, 2016, **4**, 14170–14179.
6 W. C. Cheng, C. C. Ding, Q. Y. Wu, X. X. Wang, Y. B. Sun, W. Q. Shi, T. Hayat, A. Alsaedi, Z. F. Chai and X. K. Wang, *Environ. Sci.: Nano*, 2017, **4**, 1124–1131.
7 Y. Li, L. Y. Li, T. Chen, T. Duan, W. T. Yao, K. Zheng, L. C. Dai and W. K. Zhu, *Chem. Eng. J.*, 2018, **347**, 407–414.
8 X. Liu, X. Xu, J. Sun, A. Alsaedi, T. Hayat, J. Li and X. Wang, *Chem. Eng. J.*, 2018, **343**, 217–224.
9 L. P. Lingamdinne, Y.-L. Choi, I.-S. Kim, J.-K. Yang, J. R. Koduru and Y.-Y. Chang, *J. Hazard. Mater.*, 2017, **326**, 145–156.

10 (*a*) Y. Qian, Y. Yuan, H. Wang, H. Liu, J. Zhang, S. Shi, Z. Guo and N. Wang, *J. Mater. Chem. A*, 2018, **6**, 24676–24685; (*b*) R. Ma, Y. Wang, H. Qi, C. Shi, G. Wei, L. Xiao, Z. Huang, S. Liu, H. Yu, C. Teng, H. Liu, V. Murugadoss, J. Zhang, Y. Wang and Z. Guo, *Composites, Part B*, 2019, **167**, 396–405; (*c*) K. Le, Z. Wang, F. Wang, Q. Wang, Q. Shao, V. Murugadoss, S. Wu, W. Liu, J. Liu, Q. Gao and Z. Guo, *Dalton Trans.*, 2019, **48**, 5193–5202; (*d*) A. Ahmadi, W. Yang, S. Jones and T. Wu, *Advanced Composites and Hybrid Materials*, 2018, **1**, 591–601.

11 (*a*) X. Wang, R. Li, J. Liu, R. Chen, H. Zhang, Q. Liu, Z. Li and J. Wang, *New J. Chem.*, 2017, **41**, 10899–10907; (*b*) X. Gong, Y. Liu, Y. Wang, Z. Xie, Q. Dong, M. Dong, H. Liu, Q. Shao, N. Lu, V. Murugadoss, T. Ding and Z. Guo, *Polymer*, 2019, **168**, 131–137; (*c*) Y. W. Cai, C. F. Wu, Z. Y. Liu, L. J. Zhang, L. H. Chen, J. Q. Wang, X. K. Wang, S. T. Yang and S. Wang, *Environ. Sci.: Nano*, 2017, **4**, 1876–1886; (*d*) X. Huang, R. Yin, L. Qian, W. Zhao, H. Liu, C. Liu, J. Fan, H. Hou, J. Zhang and Z. Guo, *Ceram. Int.*, 2019, DOI: 10.1016/j.ceramint.2019.05.349.

12 (*a*) G. Zhu, X. Cui, Y. Zhang, S. Chen, M. Dong, H. Liu, Q. Shao, T. Ding, S. Wu and Z. Guo, *Polymer*, 2019, **172**, 415–422; (*b*) K. Yang, J. Wang, X. Chen, Q. Zhao, A. Ghaffar and B. Chen, *Environ. Sci.: Nano*, 2018, **5**, 1264–1297; (*c*) Y. He, Q. Chen, H. Liu, L. Zhang, D. Wu, C. Lu, W. Ouyang, D. Jiang, M. Wu, J. Zhang, Y. Li, J. Fan, C. Liu and Z. Guo, *Macromol. Mater. Eng.*, 2019, DOI: 10.1002/mame.201900166.

13 S. Su, R. Chen, Q. Liu, J. Liu, H. Zhang, R. Li, M. Zhang, P. Liu and J. Wang, *Chem. Eng. J.*, 2018, **345**, 526–535.

14 X. Yang, H. Du, S. Li, Z. Wang and L. Shao, *ACS Sustainable Chem. Eng.*, 2018, **6**, 4412–4420.

15 H. Lee, S. M. Dellatore, W. M. Miller and P. B. Messersmith, *Science*, 2007, **318**, 426–430.

16 L. Li, B. Li and J. Zhang, *J. Mater. Chem. A*, 2015, **4**, 512–518.

17 X. Yang, Z. Wang and L. Shao, *J. Membr. Sci.*, 2018, **549**, 67–74.

18 Z. W. Huang, Z. J. Li, Q. Y. Wu, L. R. Zheng, L. M. Zhou, Z. F. Chai, X. L. Wang and W. Q. Shi, *Environ. Sci.: Nano*, 2018, **5**, 2077–2087.

19 P. Yang, Q. Liu, J. Liu, H. Zhang, Z. Li, R. Li, L. Liu and J. Wang, *J. Mater. Chem. A*, 2017, **5**, 17933–17942.

20 P. Yang, Q. Liu, H. Zhang, J. Liu, R. Chen, R. Li, D. Wu, X. Bai and J. Wang, *Environ. Sci.: Nano*, 2018, **5**, 1584–1594.

21 W. S. Hummers and R. E. Offeman, *J. Am. Chem. Soc.*, 1958, **80**, 1339.

22 Z. Q. Bai, L. Y. Yuan, L. Zhu, Z. R. Liu, S. Q. Chu, L. R. Zheng, J. Zhang, Z. F. Chai and W. Q. Shi, *J. Mater. Chem. A*, 2015, **3**, 525–534.

23 V. Jabbari, J. M. Veleta, M. Zarei-Chaleshtori, J. Gardea-Torresdey and D. Villagrán, *Chem. Eng. J.*, 2016, **304**, 774–783.

24 W. Cui, M. Li, J. Liu, B. Wang, C. Zhang, L. Jiang and Q. Cheng, *ACS Nano*, 2014, **8**, 9511–9517.

25 J. Yang, D. Shen, Y. Wei, W. Li, F. Zhang, B. Kong, S. Zhang, W. Teng, J. Fan, W. Zhang, S. Dou and D. Zhao, *Nano Res.*, 2015, **8**, 2503–2514.

26 Z.-Y. Xi, Y.-Y. Xu, L.-P. Zhu, Y. Wang and B.-K. Zhu, *J. Membr. Sci.*, 2009, **327**, 244–253.

27 R.-H. Lin and J.-H. Hsu, *Polym. Int.*, 2001, **50**, 1073–1081.

28 X. Li, T. Liu, D. Wang, Q. Li, Z. Liu, N. Li, Y. Zhang, C. Xiao and X. Feng, *ACS Appl. Mater. Interfaces*, 2018, **10**, 21672–21680.

29 F. Yuan, C. Wu, Y. Cai, L. Zhang, J. Wang, L. Chen, X. Wang, S. Yang and S. Wang, *Chem. Eng. J.*, 2017, **322**, 353–365.

30 M. J. Manos and M. G. Kanatzidis, *J. Am. Chem. Soc.*, 2012, **134**, 16441–16446.

31 C. Mizuno, S. H. Bao, T. Hinoue and T. Nomura, *Anal. Sci.*, 2005, **21**, 281–286.

32 R. D. Shannon, *Acta Crystallogr., Sect. A: Cryst. Phys., Diffr., Theor. Gen. Crystallogr.*, 1976, **32**, 751–767.

33 A. C. Sutorik and M. G. Kanatzidis, *J. Am. Chem. Soc.*, 1997, **119**, 7901–7902.

34 L. Li, W. Ma, S. Shen, H. Huang, Y. Bai and H. Liu, *ACS Appl. Mater. Interfaces*, 2016, **8**, 31032–31041.

35 S. Duan, Y. Wang, X. Liu, D. Shao, T. Hayat, A. Alsaedi and J. Li, *ACS Sustainable Chem. Eng.*, 2017, **5**, 4073–4085.

36 Y. Peng, H. Huang, D. Liu and C. Zhong, *ACS Appl. Mater. Interfaces*, 2016, **8**, 8527–8535.

37 Y. Sun, X. Wang, Y. Ai, Z. Yu, W. Huang, C. Chen, T. Hayat, A. Alsaedi and X. Wang, *Chem. Eng. J.*, 2017, **310**, 292–299.

38 F. You, Y. Xu, X. Yang, Y. Zhang and L. Shao, *Chem. Commun.*, 2017, **53**, 6128–6131.

39 T. Zheng, Z. Yang, D. Gui, Z. Liu, X. Wang, X. Dai, S. Liu, L. Zhang, Y. Gao, L. Chen, D. Sheng, Y. Wang, J. Diwu, J. Wang, R. Zhou, Z. Chai, T. E. Albrecht-Schmitt and S. Wang, *Nat. Commun.*, 2017, **8**, 15369.

40 Y. Sun, X. Wang, W. Song, S. Lu, C. Chen and X. Wang, *Environ. Sci.: Nano*, 2017, **4**, 222–232.

41 Y. Ai, Y. Liu, W. Lan, J. Jin, J. Xing, Y. Zou, C. Zhao and X. Wang, *Chem. Eng. J.*, 2018, **343**, 460–466.

42 A. L. Yang, J. H. Wu and C. P. Huang, *J. Hazard., Toxic Radioact. Waste*, 2018, **22**, 04017029.

43 H. H. El-Maghrabi, S. M. Abdelmaged, A. A. Nada, F. Zahran, S. A. El-Wahab, D. Yahea, G. M. Hussein and M. S. Atrees, *J. Hazard. Mater.*, 2017, **322**, 370–379.

44 L. C. Tan, Y. L. Wang, Q. Liu, J. Wang, X. Y. Jing, L. H. Liu, J. Y. Liu and D. L. Song, *Chem. Eng. J.*, 2015, **259**, 752–760.

45 N. Pan, L. Li, J. Ding, S. Li, R. Wang, Y. Jin, X. Wang and C. Xia, *J. Hazard. Mater.*, 2016, **309**, 107–115.

46 L. Shao, X. F. Wang, Y. M. Ren, S. F. Wang, J. R. Zhong, M. F. Chu, H. Tang, L. Z. Luo and D. H. Xie, *Chem. Eng. J.*, 2016, **286**, 311–319.